Electronic Supplementary Material (ESI) for ChemComm.
This journal is © The Royal Society of Chemistry 2018

Supporting Information

Excitation-Wavelength-Dependent Photoluminescence of Silicon Nanoparticles Enabled by Adjustment of Surface Ligands

Xiao-Bin Shen,[¶,§] Bin Song,[‡,§] Bei Fang,[‡] Ai-Rui, Jiang,[‡] Shun-Jun Ji,*[,¶] and Yao He*,[‡]

[¶] Key Laboratory of Organic Synthesis of Jiangsu Province, College of Chemistry, Chemical Engineering and Materials Science, Soochow University, Suzhou 215123, China

[‡] Jiangsu Key Laboratory for Carbon-Based Functional Materials and Devices, Institute of Functional Nano and Soft Materials (FUNSOM) and Collaborative Innovation Center of Suzhou Nano Science and Technology (NANO-CIC), Soochow University, Suzhou 215123, China

E-mail: shunjun@suda.edu.cn; yaohe@suda.eud.cn;

Additional Experimental Methods and Data

1. Experimental methods

1.1. Materials and Devices.

All chemicals were purchased from Sigma-Aldrich without additional purification. The ligand-synthesizing reactions were monitored by thin-layer chromatography (TLC) on silica gel GF-254 precoated glass plates. Chromatograms were visualized by UV light at 254 nm. Flash column chromatography was performed using silica gel. ^{1}H and ^{13}C NMR spectra were recorded in $CDCl_3$ or D_6-DMSO on 400 MHz spectrometers. Tetramethylsilane (TMS) served as internal standard for ^{1}H NMR, $CDCl_3$ or D_6-DMSO was used as internal standard for ^{13}C NMR. HRMS was recorded on a commercial apparatus (ESI Source). All solutions were prepared using Milli-Q water (Millipore) as the solvent when preparing SiNPs. The microwave system NOVA-2S used for synthesizing SiNPs was made by Preekem of Shanghai, China. Exclusive vitreous vessels with a volume of 15 or 20 mL are equipped for the system to provide security during reaction demanding high temperature and pressure. The SiNPs were characterized by UV-vis absorption, photoluminescence (PL), transmission electronic microscopy (TEM), high-resolution TEM (HRTEM), Fourier-transform infrared (FT-IR) spectroscopy, energy dispersive X-ray spectroscopy (EDX), and X-ray photoemission spectroscopy (XPS). Optical measurements were performed at room temperature under ambient air conditions. UV-vis absorption spectra were recorded with a Perkin-Elmer lambda 750 UV-vis near-infrared spectrophotometer. 600 μL solution of the as-prepared SiNPs sample was transferred into an exclusive quartz cuvette for UV spectra measurements. PL measurements were performed using a HORIBA JOBIN YVON FLUOROMAX-4 spectrofluorimeter. The photoluminescent quantum yield (PLQY) was estimated using Quinine Sulfate (literature quantum yield: 58%) as a reference standard, which was freshly prepared with aim to reduce the measurement error. TEM and HRTEM samples were prepared by dispersing the sample onto carbon-coated copper grids with the excess solvent evaporated. The TEM/HRTEM overview images were recorded using Philips CM 200 electron microscope operated at 200 kV. For FT-IR measurements, KBr was pressed into a slice, onto which the SiNPs sample was dropped. The solvent in the sample was adequately evaporated by irradiation (> 30 min) with a high-power incandescent lamp. FT-IR spectra were recorded on a Bruker HYPERION FT-IR spectrometer and cumulated 32 scans at a resolution of 4 cm^{-1}.

Light-scattering analysis was performed using a DynaPro dynamic light scatterer (DLS), which was made by Malvern Corp, U.K. (ZEN3690). 1 mL SiNPs aqueous solution was transferred into an exclusive vitreous (container) for DLS measurements. Experiment parameters were as follows: scan times: 100; dispersant: water; temperature: 25 °C; viscosity: 0.8872 cP; RI: 1.330; and dielectric constant: 78.5. EDX spectroscopy was utilized to determine the fraction of the resultant SiNPs. The SiNPs samples were first dispersed onto carbon-coated copper grids with the excess solvent evaporated and then characterized by using Philips CM 200 electron microscope, equipped with EDX spectroscopy. High-resolution XPS analyses were performed using a Kratos AXIS Ultra^{DLD} ultrahigh vacuum (UHV) surface analysis system, which consists of a fast entry air lock (base pressure $<1 \times 10^{-8}$ Torr), a multiport carousel chamber ($<5 \times 10^{-10}$ Torr), a deposition chamber ($<5 \times 10^{-10}$ Torr), and an analysis chamber ($<3 \times 10^{-10}$ Torr). A monochromatic Al Kα source (1486.6 eV) with a resolution of 0.5 eV was used to irradiate the samples. The spectra were internally calibrated to the C 1s emission (284.8 eV). After calibration, the background was subtracted using a Shirley-type background to remove most of the extrinsic loss structure. Time-resolved lifetime curve was performed using a HORIBA JOBIN YVON FL-TCSPC fluorescence spectrometer. The probe beam was a 370 nm or 450 nm laser beam (with a repetition frequency of 1 MHz). Anti-counterfeiting patterned images were captured by a Maestro in vivo optical imaging system (Cambridge Research & instrumentation, Inc.) equipped with diode laser 360 nm, 455 nm and 523 nm. Multi-color bioimaging was examined under a confocal laser microscope (Leica, TCS-SP5) equipped with diode laser 405 nm, 458 nm and 514 nm. Images were captured and processed with image analysis software.

1.2 Design and synthesis of surface ligands

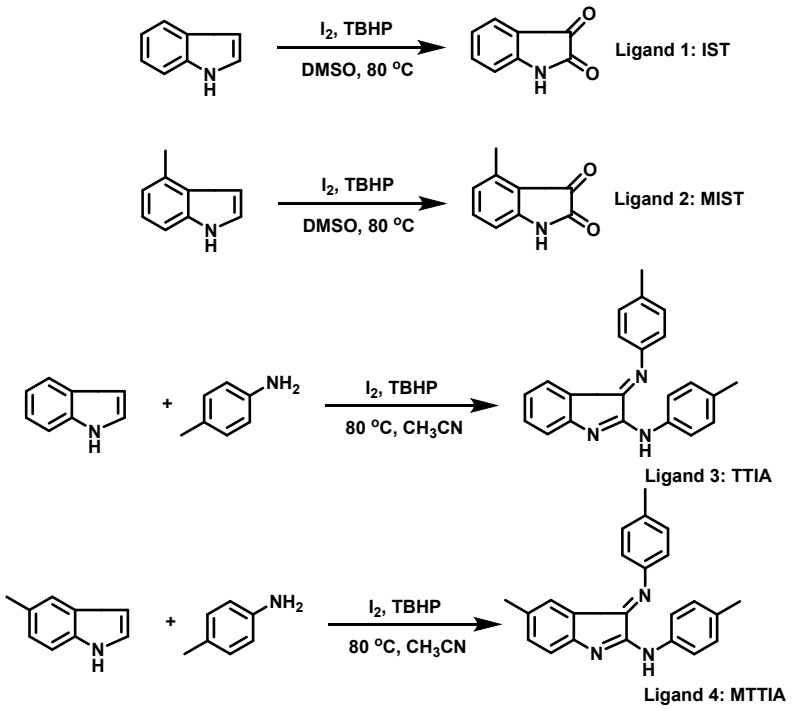

Scheme S1. The passivation reactions of indole molecules through I_2/TBHP mediated approach. The indole molecules can be conveniently converted into their oxidized derivatives through oxidation reactions, which can be further utilized as the surface ligands for formation of ligand-decorated SiNPs.

Synthesis of the oxidized indole derivatives Ligand 1 and 2 were synthesized via similar procedure: under ambient air condition, substrate indole (2 mmol) and DMSO (2 mL) were added into a flask and stirred vigorously at 80 °C. Then the mixture of I_2 (2.4 mmol, 0.6092 g), TBHP (70% aq., 5 equiv., 5 mmol), and DMSO (6 mL) was added into the flask dropwise. The reaction was stopped until substrate indole was completely consumed, which was monitored by TLC analysis. The reaction was quenched by $Na_2S_2O_3$ solution (5% aq., 10 mL), and further extracted with water and EtOAc. The organic solution was dried with Na_2SO_4, and then evaporated under vaccum. The residue was purified by column chromatography on silica gel to afford the desired products. (Note: Ligand 1-IST is commercially available, so the NMR profile of L1 is not provided herein.)

Ligand 3 and 4 were synthesized via similar procedure: the substrate indole (5 mmol), *p*-toluidine (20 mmol, 2.1425 g), I_2 (0.5 mmol, 0.1270 g, 10 mol%), and acetonitrile (5 mL) were added into a 50-mL flask, then TBHP (70% aq., 6 equiv., 6 mmol) was added into the flask dropwise. The system was stirred at 40 °C. The reaction was monitored by TLC analysis until substrate indole was completely consumed. After that, the reaction was quenched by $Na_2S_2O_3$ solution (5% aq., 10 mL). The mixture was extracted with water and EtOAc. The organic solution was dried with Na_2SO_4, and then the solvent was removed by vaccum evaporation. The residue was purified

by column chromatography on silica gel to afford the desired products.

Characterization Data of Organic Compounds

4-methylindoline-2,3-dione (Ligand 2)

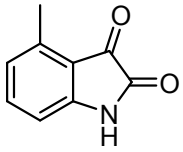

^{1}H NMR (400 MHz, DMSO-d_6) (δ, ppm): 10.99 (s, 1H), 7.44 (t, J = 7.8 Hz, 1H), 6.86 (d, J = 7.7 Hz, 1H), 6.71 (d, J = 7.8 Hz, 1H), 2.44 (s, 3H).

^{13}C NMR (101 MHz, DMSO-d_6) (δ, ppm): 184.86, 159.09, 150.74, 139.58, 137.80, 124.73, 115.81, 109.48, 40.12, 39.91, 39.70, 39.50, 39.29, 39.08, 38.87, 17.40. (Details can be seen in Figure S2)

HRMS (ESI) m/z: Found: 162.0554. Calcd for $C_9H_7NO_2$: $(M+H)^+$ 162.0555.

(*E*)-*N*-(*p*-tolyl)-3-(*p*-tolylimino)-3*H*-indol-2-amine (Ligand 3)

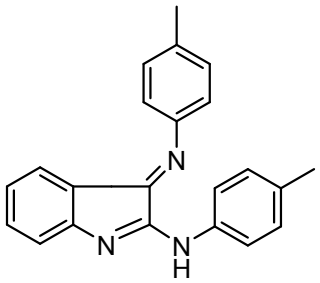

^{1}H NMR (400 MHz, $CDCl_3$) (δ, ppm): 7.89 (s, 1H), 7.74 (d, J = 8.0 Hz, 2H), 7.26 – 7.19 (m, 6H), 6.98 (d, J = 8.2 Hz, 2H), 6.78 (d, J = 7.4 Hz, 1H), 6.65 (td, J = 7.4Hz, 1H), 2.42 (s, 3H), 2.35 (s, 3H).

^{13}C NMR (101 MHz, $CDCl_3$) (δ, ppm): 146.15, 135.89, 135.46, 134.36, 133.04, 129.93, 129.75, 125.51, 122.41, 119.15, 119.03, 77.32, 77.00, 76.68, 21.08, 20.92. (Details can be seen in Figure S3).

HRMS (ESI) m/z: Found: 326.1666. Calcd for $C_{22}H_{19}N_3$: $(M+H)^+$ 326.1657.

(*E*)- 6-methyl-N-(*p*-tolyl)-3-(*p*-tolylimino)-3*H*-indol-2-amine (Ligand 4)

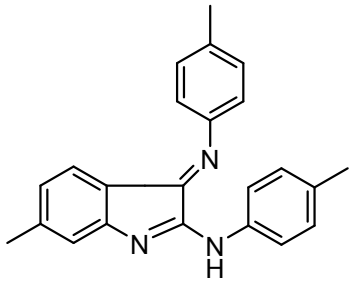

^{1}H NMR (400 MHz, $CDCl_3$) (δ, ppm): 7.89 (s, 1H), 7.73 (d, J = 7.8 Hz, 2H), 7.21 (dd, J = 16.4, 7.9 Hz, 4H), 6.98 (t, J = 10.2 Hz, 3H), 6.67 (d, J = 7.6 Hz, 1H), 6.45 (d, J = 7.6 Hz, 1H), 2.41 (s, 3H), 2.34 (s, 3H), 2.28 (s, 3H).

^{13}C NMR (101 MHz, $CDCl_3$) (δ, ppm): 145.89, 145.09, 134.78, 132.51, 129.42, 129.26, 124.89, 122.49, 119.49, 118.69, 76.88, 76.56, 76.24, 21.72, 20.61, 20.45. (Details can be seen in Figure S4).

HRMS (ESI) m/z: Found: 340.1823. Calcd for $C_{23}H_{21}N_3$: $(M+H)^+$ 340.1814.

1.3 Synthesis of SiNPs

Synthesis of NH_2-capped SiNPs. Microwave-assisted synthesis is utilized in our experiment based on our previous experience in the synthesis of silicon nanomaterials.[1,2] In details, trisodium citrate (0.4 g) was added into a 50-mL round-bottom flask, which was dissolved by 8 mL Milli-Q water. Then 2 mL of (3-aminopropyl) trimethoxysilane (APTMS) was added into the flask dropwise. The mixture was stirred for 10 min. This precursor solution was transferred into a 30-mL

exclusive vitreous vessel. After 30-min microwave reaction at 160 °C, the sample was collected when the temperature cooled to < 30 °C naturally. Dialysis (1 kDa) was used to purify the obtained sample. The purified aqueous solution was further dried over vacuum to afford pure NH_2-capped SiNPs as a white powder.[3]

Synthesis of ligand-decorated SiNPs. The as-prepared NH_2-capped SiNPs solid (2.00 g) was re-dispersed in 10 mL Milli-Q water. The as-prepared ligand (~20 mg) was added into the mixture, then ligand decoration was completed in a 30-min microwave reaction at 160 °C. The resultant solution was collected when it was cooled to lower than 30 °C. Next, to purify the as-prepared ligand-decorated SiNPs, the obtained solution was centrifuged for 10 min at 8000 rpm, the precipitate, which was composed of unreactive ligand and unsolvable big-sized silicon hybrid, was discarded. The supernatant was further purified by ultrafiltration to fully remove the excess organic byproducts. Usually, ultrafiltration with centrifugal filters Pall Nanosep 30 kDa from Millipore was carried out with the big-size particles remained in the upper layer, and small-sized particles were transferred to the lower layer. The lower layer solution was further ultrafiltrated with 10 kDa centrifugal filters to fully remove the organic byproduct and inorganic salts. Finally, the solvent was removed through rotary-vaccum evaporation, and the pale solid of SiNPs was thus obtained. The purified SiNPs were then used for following characterizations and applications.

1.4 Preparation of SiNPs-composed security ink and anti-counterfeiting imaging

The prepared IST-SiNPs solid was re-dispersed into water to prepare 3.0 mg/mL SiNPs-solution, which was then used as a security ink. Similarly, commercially available R6G (yellow) fluorescent ink (0.3 mg/mL) was prepared. The cartridge of an inkjet printer was filled with the prepared inks. A common printer was used for printing the desired images. A Maestro in vivo optical imaging system (Cambridge Research & instrumentation, Inc.) was utilized for imaging the printed patterns. In particular, the fluorescent images were captured under the following conditions: excitation wavelength: 360 nm, blue emission window: 460-490 nm, exposure time: 800 ms; excitation wavelength: 455 nm, green emission window: 490-520 nm, exposure time: 2000 ms; excitation wavelength: 523 nm, yellow emission window: 540-590 nm, exposure time: 5000 ms.

1.5 Fluorescence Imaging *in Vitro*

The prepared SiNPs (IST-SiNPs were employed as a model) were used for fluorescence labeling of fixed HeLa cells. Human epithelial cervical cancer cells (HeLa cells) were cultured (37 °C, 5% CO_2) on cover glass in Dulbecco's modified Eagle's medium with 10% heatinactivated fetal bovine serum and antibiotics (100 μg/mL streptomycin and 100 U/ml penicillin) overnight. HeLa cells were fixed with 4% paraformaldehyde for 20 min and blocked for 40 min in PBS containing 4% BSA and 0.1% Triton X-100. Fixed and blocked HeLa cells were incubated sequentially with materials for 12 h. The stained cells were mounted on slides in fluoromount (Sigma, F4680) with coverslips.

Multi-color bioimaging was examined under a confocal laser microscope (Leica, TCS-SP5) equipped with diode laser 405 nm, 458 nm and 514 nm. Images were captured and processed with image analysis software. In particular, the fluorescent cell images were captured under the following parameters: excitation wavelength: 405 nm, emission band pass: 430-470 nm; excitation wavelength: 458 nm, emission band pass: 470-510 nm; excitation wavelength: 514 nm, emission band pass: 530-570 nm.

1.6 Photoluminescent quantum yields (PLQY) measurements

In our experiment, a well-established method was employed for determining the PLQY of SiNPs as follow (quinine sulfate in 0.1 M H_2SO_4 (literature quantum yield: 58%)):[4]

$$\Phi_x=\Phi_{st}\,(K_x/K_{st})\,(\eta_x/\eta_{st})^2$$

Where Φ is quantum yield, "*K*" is the slope of curves, and "η" is the refractive index of the solvent (equal to 1.0 in our case)[5]. The subscript "st" refers to the referenced fluorophore (quinine sulfate in 0.1 M H_2SO_4) with known QY, and "x" refers as the SiNPs sample, respectively. To minimize reabsorption effects, absorption value is kept below 0.10.

2. Additional Data

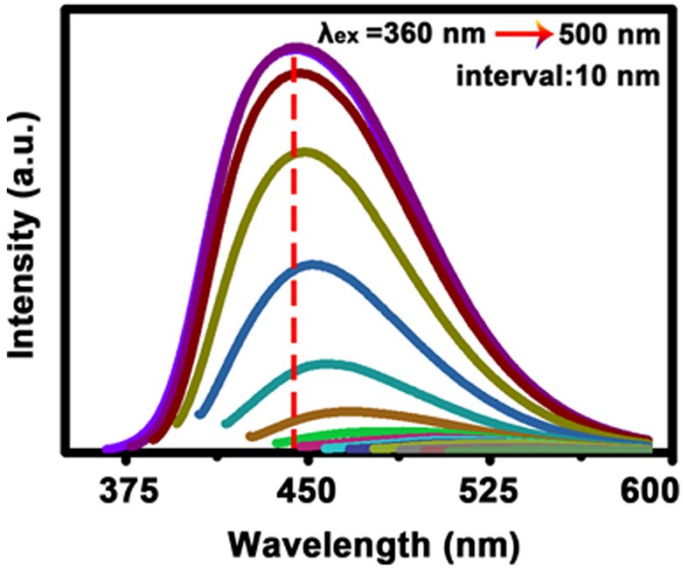

Fig. S1 PL spectra of indole-decorated SiNPs under different excitation wavelengths. The spectra show that with the excitation wavelength increases from 360 to 500 nm, the redshift of the emission peak can hardly be observed. This result proves that surface modification with indole molecule produces little influence on the maximum emission wavelength of SiNPs.

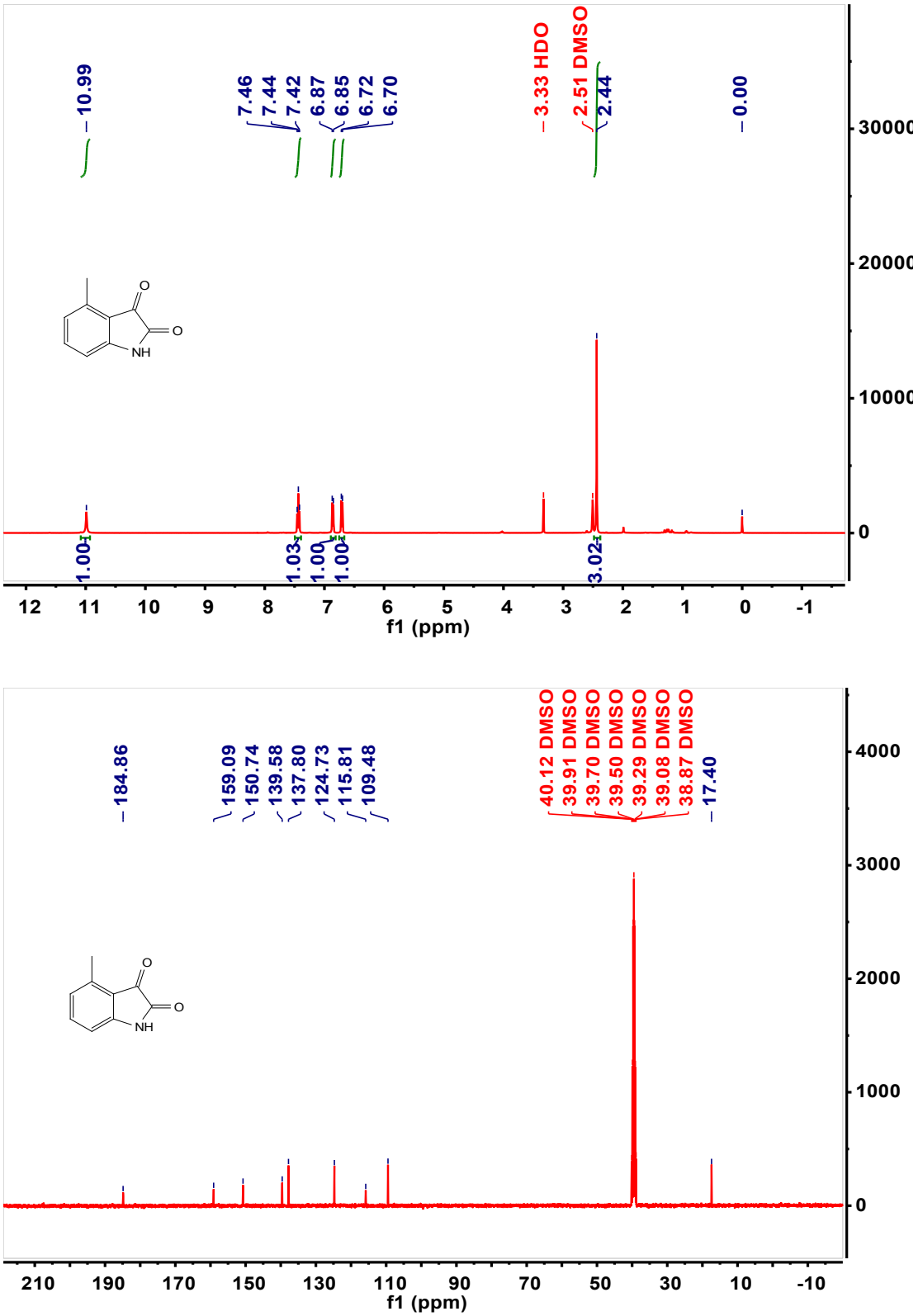

Fig. S2 ^{1}H and ^{13}C NMR spectrum of **Ligand 2** (MIST). The detail split data and coupling constant was fully organized in part 1.2. The spectrum shows good purity of this compound for the further use in the decoration of SiNPs.

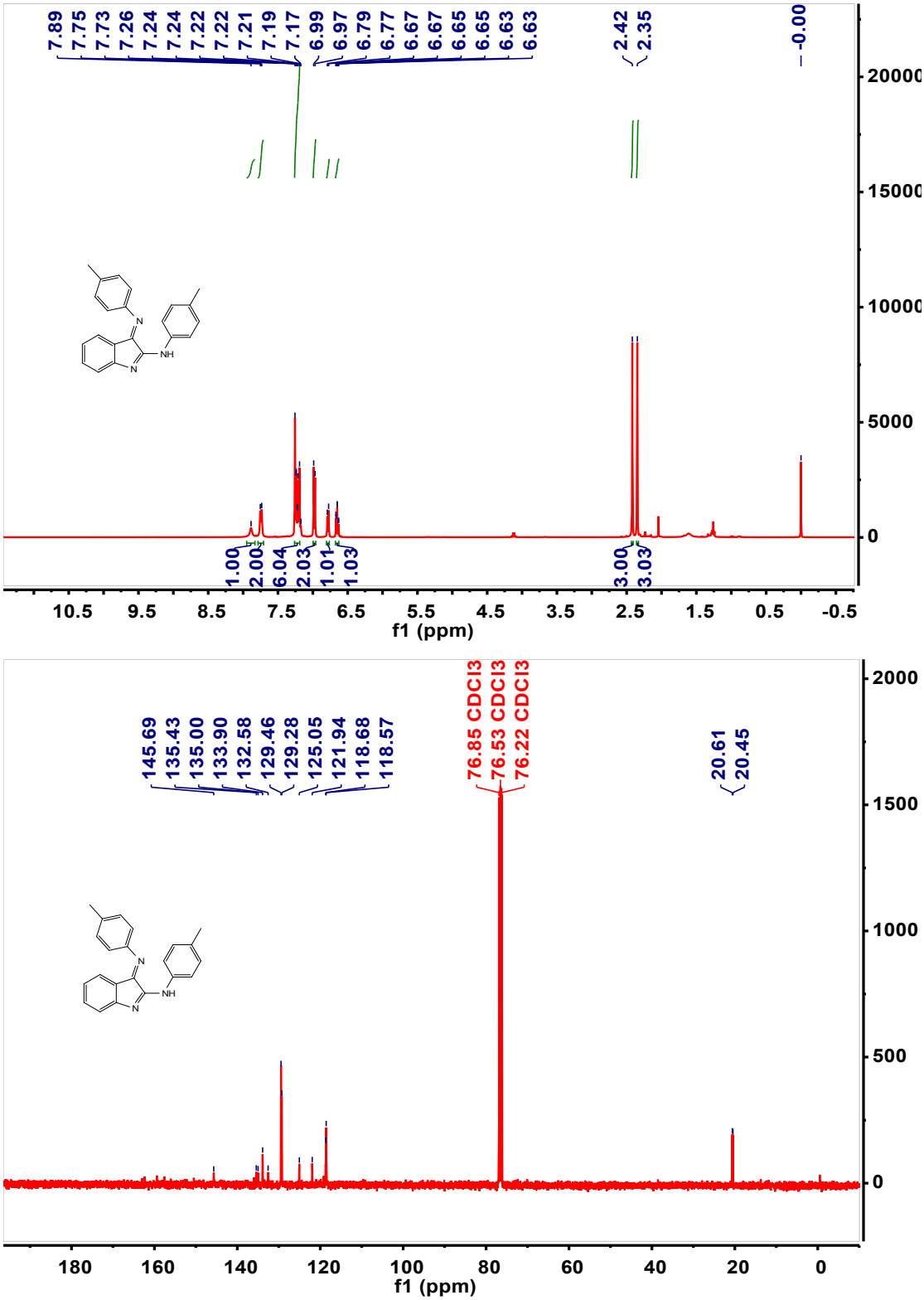

Fig. S3 ^{1}H and ^{13}C NMR spectrum of **Ligand 3** (TTIA). The detail split data and coupling constant was fully organized in part 1.2. The spectrum shows good purity of this compound for the further use in the decoration of SiNPs.

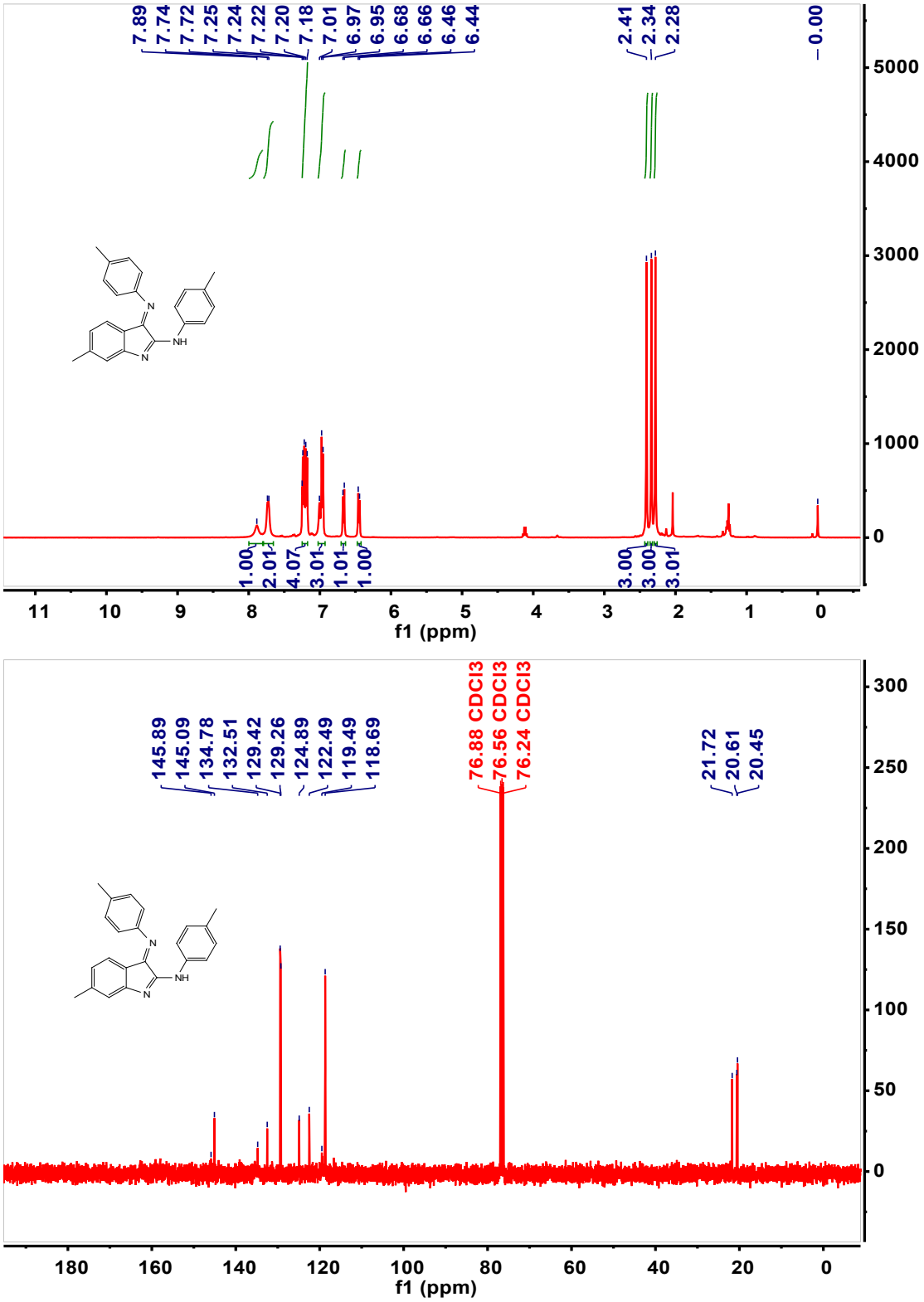

Fig. S4 ^{1}H and ^{13}C NMR spectrum of **Ligand 4** (MTTIA). The detail split data and coupling constant was fully organized in part 1.2. The spectrum shows good purity of this compound for the further use in the decoration of SiNPs.

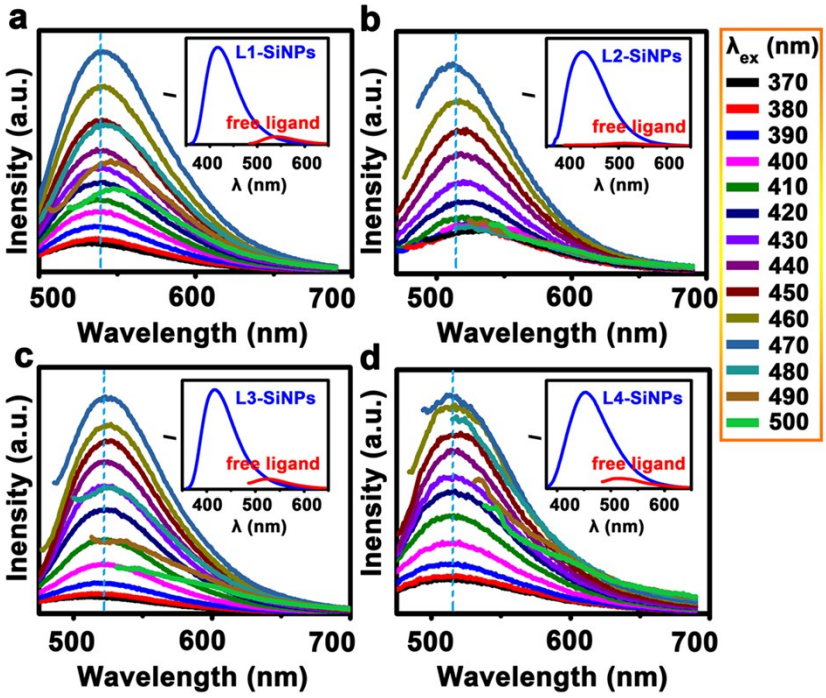

Fig. S5 PL spectra of free ligands treated by microwave irradiation under different excitation wavelengths: (a) L1-IST; (b) L2-MIST; (c) L3-TTIA; (d) L4-MTTIA. The resultant materials exhibit excitation-wavelength-independent PL property, with an emission peak at ~530 nm. And also, the resultant materials show feeble fluorescence compared with ligand-decorated SiNPs (insert). Furthermore, the maximum emission wavelengths of these materials are coincided with the corresponding ligand-decorated SiNPs excited at ~450 nm. These results provide firm evidence that the green luminescence of SiNPs is produced by the radiative recombination of excitons in the localized gap in the ligand layer

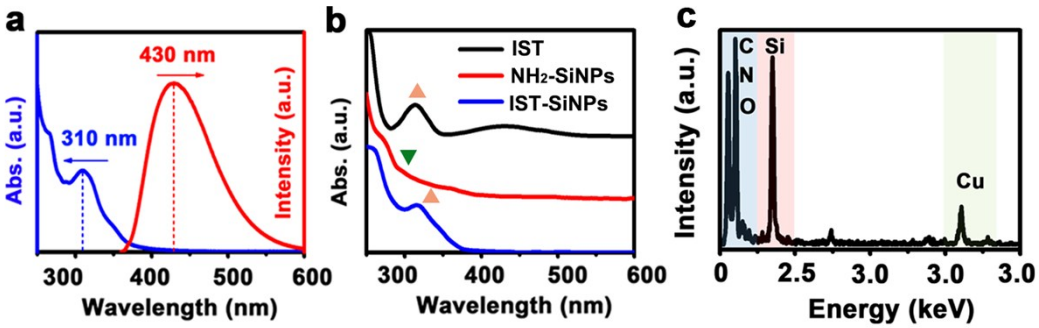

Fig. S6 (a) Normalized UV-PL spectra of IST-SiNPs (for PL spectrum, λ_{ex} = 370 nm). (b) UV-vis spectra of free IST, NH_2-SiNPs, and IST-SiNPs. The absorption spectrum of IST-SiNPs shows a distinct peak at ~310 nm, which is different from that of NH_2-SiNPs. This newly generated electronic transition is mainly attributed to the ligand, since the absorption spectra on ligand also displays an evident peak at ~310 nm. (c) EDX spectrum: the EDX spectrum reveals that the resultant SiNPs mainly contain Si located in ~1.73 keV. Whereas a significant C peak located in ~0.27 keV is also observed, indicating there is a large amount of C contained in the sample. This high content of carbon is mainly originated from two parts, i.e., carbon-coated copper girds and surface ligand attached to the SiNPs. N and O peaks are also detectable at ~0.39 keV and ~0.52 keV, showing the existence of $–NH_2$, –NL, and oxide layer, which is consisted with the results from Fourier-transform infrared (FT-IR) spectra and X-ray photoemission spectra (XPS) of the resultant SiNPs.

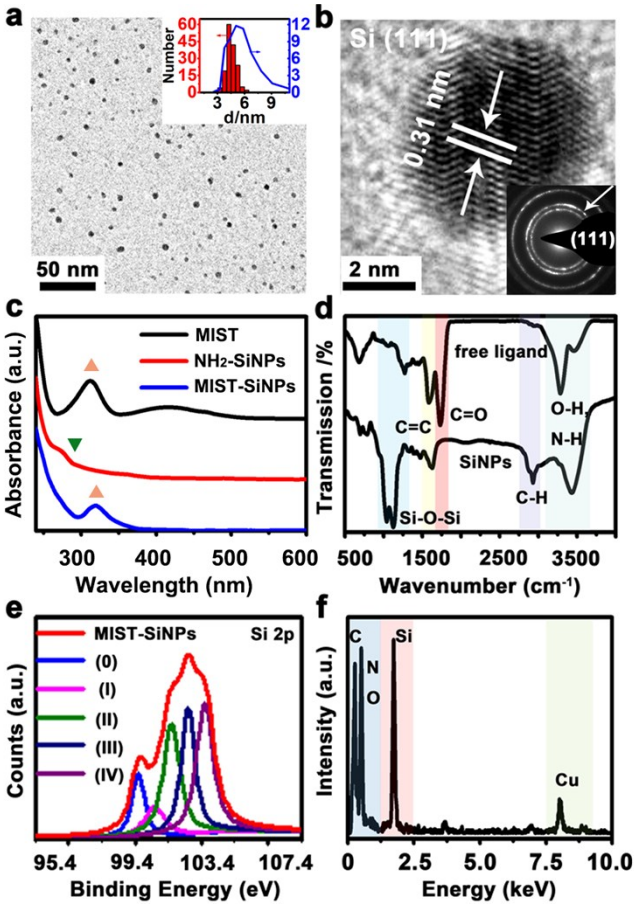

Fig. S7 Characterizations data for the MIST-SiNPs. (a) TEM image of the MIST-SiNPs. The TEM result indicates good monodispersity of the prepared SiNPs. The inset shows the TEM size deviation (4.2 ± 0.5 nm) and DLS diameter (~5.3 nm) of the SiNPs: the size distribution is measured over 300 particles; the different result from TEM size distribution and DLS diameter is due to distinct surface conditions of the SiNPs samples under the different measurement environment.[3] (b) HRTEM image of a single SiNP; the insert shows selected-area electron diffraction pattern. Clear lattice spacing of ~0.31 nm for a single SiNP is observed, which corresponds to the (111) facet of Si, consistent with the lattice spacing measured through electron diffraction. These results suggest good crystallinity of these SiNPs. (c) UV-vis spectra of free MIST, NH_2-SiNPs, and MIST-SiNPs: ~310 nm absorption peak is observed for both free MIST and MIST-SiNPs, but absent for NH_2-SiNPs. (d) FT-IR spectra of free ligand and corresponding SiNPs. The characteristic C=C stretch (*ca.* ~1652 cm^{-1}) is observed in the spectra of neat ligand and SiNPs, providing firm evidence for the successful decoration of SiNPs. Besides, the strong and sharp absorbance peak at ~1030 cm^{-1} attributed by Si-O-Si suggests the high oxidation state of SiNPs. (e) X-ray photoemission spectra of Si 2p region displays the band can be deconvoluted into five peaks, corresponding to Si(0), Si(I), Si(II), Si(III) and Si(IV), at 99.4 eV, 100.4 eV, 101.4 eV, 102.4 eV and 103.4 eV, respectively. The appearance of the Si(0) signal confirms the existence of a silicon core. Besides, the strong signals of Si(III) and Si(IV) can be observed, indicating the high oxidation state of Si, which is coincided with the result of FT-IR. (f) EDX spectrum reveals the existence of Si, C, O, and N within the nanoparticle. The characterization results indicate crystalline Si/SiO_xN_y core/shell structure of SiNPs, whose surface is covered by MIST ligands.

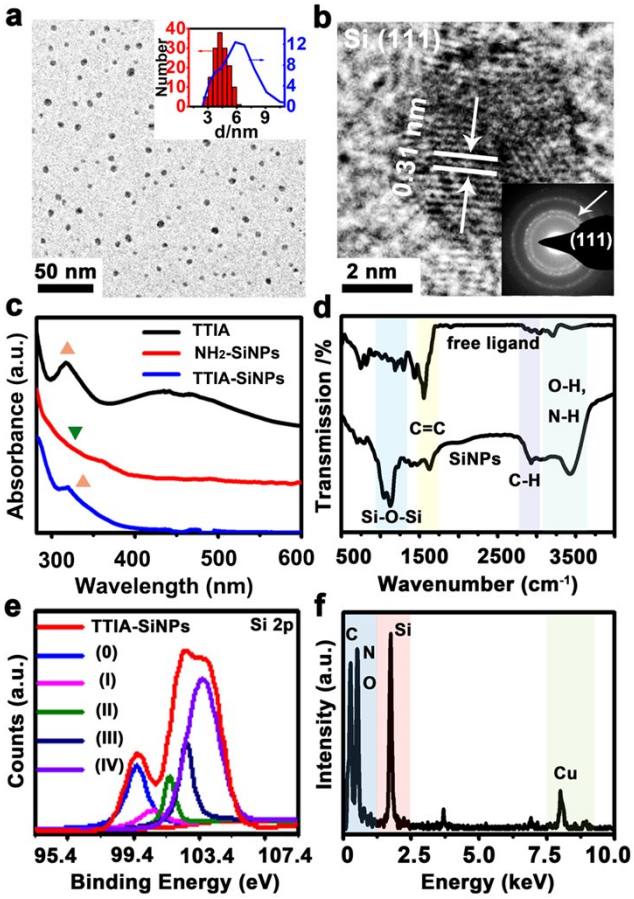

Fig. S8 Characterization data for the TTIA-SiNPs. (a) TEM image of the TTIA-SiNPs. The TEM result indicates good monodispersity of these SiNPs. The inset shows the TEM size deviation (4.2 ± 0.6 nm) and DLS diameter (~5.8 nm) of the SiNPs. (b) HRTEM image of a single SiNP; the insert shows selected-area electron diffraction pattern. Clear lattice spacing of ~0.31 nm for a single SiNP is observed, which corresponds to the (111) facet of Si, consistent with the lattice spacing measured through electron diffraction. These results suggest good crystallinity of these SiNPs. (c) UV-vis spectra of free TTIA, NH_2-SiNPs, and TTIA-SiNPs: ~320 nm absorption peak is observed for both free TTIA and TTIA-SiNPs, but undetectable for NH_2-SiNPs, indicating the newly formed electronic transition at ~320 nm in TTIA-SiNPs is originated from ligand. (d) FT-IR spectra demonstrate the attachment of ligand on the surface of SiNPs: Si-OH and $–NH_2$ vibrations at 3200-3600 cm^{-1}, aromatic C-H bands at 2850-3100 cm^{-1}, C=C stretch at ~1650 cm^{-1}, and Si-O-Si vibrations at ~1045 cm^{-1} can be observed, suggesting successful decoration and high oxidation state of SiNPs. (e) X-ray photoemission spectra of Si 2p region: five resolved peaks can be deconvoluted for the band, corresponding to Si(0), Si(I), Si(II), Si(III) and Si(IV), at 99.4, 100.4, 101.4, 102.4 and 103.4 eV, respectively. The appearance of Si(III) and Si(IV) signals indicates the high oxidation state of these SiNPs, which is coincided with the result of FT-IR. (f) EDX spectrum reveals the existence of Si, C, O, and N within the nanoparticle. The characterization results suggest crystalline Si is embedded in a SiO_xN_y shell, whose surface is covered by TTIA ligand.

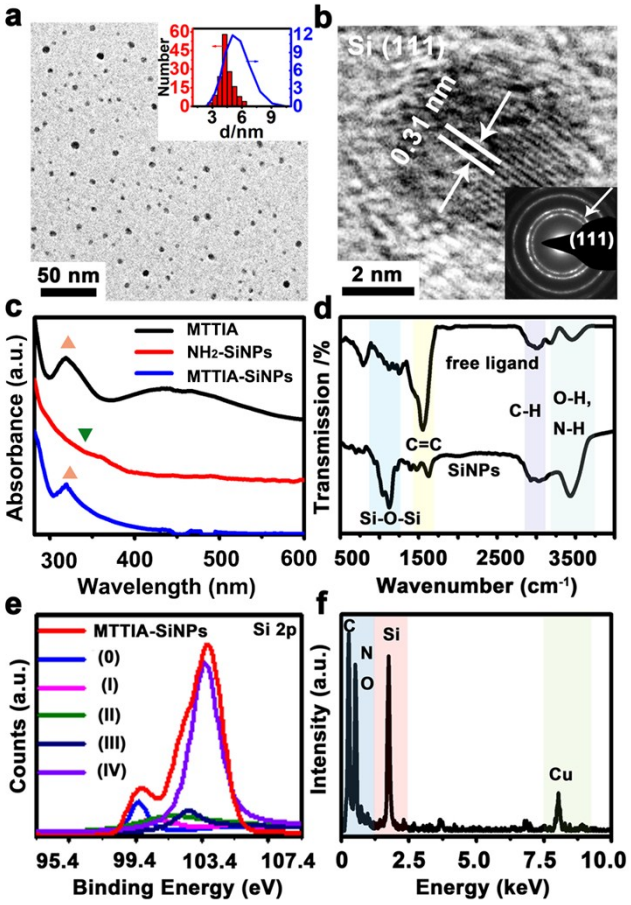

Fig. S9 Characterization data for the MTTIA-SiNPs. (a) TEM image of the MTTIA-SiNPs. The TEM result indicates good monodispersity of these SiNPs. The inset shows the TEM size deviation (4.3 ± 0.7 nm) and DLS diameter (~5.1 nm) of the SiNPs. (b) HRTEM image of a single SiNP; the insert shows selected-area electron diffraction pattern. Clear lattice spacing of ~0.31 nm for a single SiNP is observed, which corresponds to the (111) facet of Si, consistent with the lattice spacing measured through electron diffraction. These results suggest good crystallinity of these SiNPs. (c) UV-vis spectra of free MTTIA, NH_2-SiNPs, and MTTIA-SiNPs: ~320 nm absorption peak is observed for both free MTTIA and MTTIA-SiNPs, but undetectable for NH_2-SiNPs. (d) FT-IR spectra of free ligand and corresponding SiNPs show similar vibration signals with that of TTIA-SiNPs. In particular, characteristic C=C stretch (*ca.* ~1638 cm^{-1}) appears in both of the spectra of neat ligand and SiNPs, providing firm evidence of successful decoration. Furthermore, high oxidation Si-O-Si vibration at ~ 1040 cm^{-1} can also be observed. (e) X-ray photoemission spectra of Si 2p band for MTTIA-SiNPs can be deconvoluted into five peaks, in which Si(0), Si(I), Si(II), Si(III), and Si(IV) at 99.4, 100.4, 101.4, 102.4, and 103.4 eV, respectively, can be observed. The strong signals arisen from Si(III) and Si(IV) indicate the high oxidation state of Si. This result is coincided with FT-IR. (f) EDX spectrum confirms the high content of Si within the nanoparticles. The characterization result indicates the similar nanoparticle structure with other three kinds of ligand-decorated SiNPs, i.e., crystalline Si core/SiO_xN_y shell-structure particle is covered by MTTIA ligands.

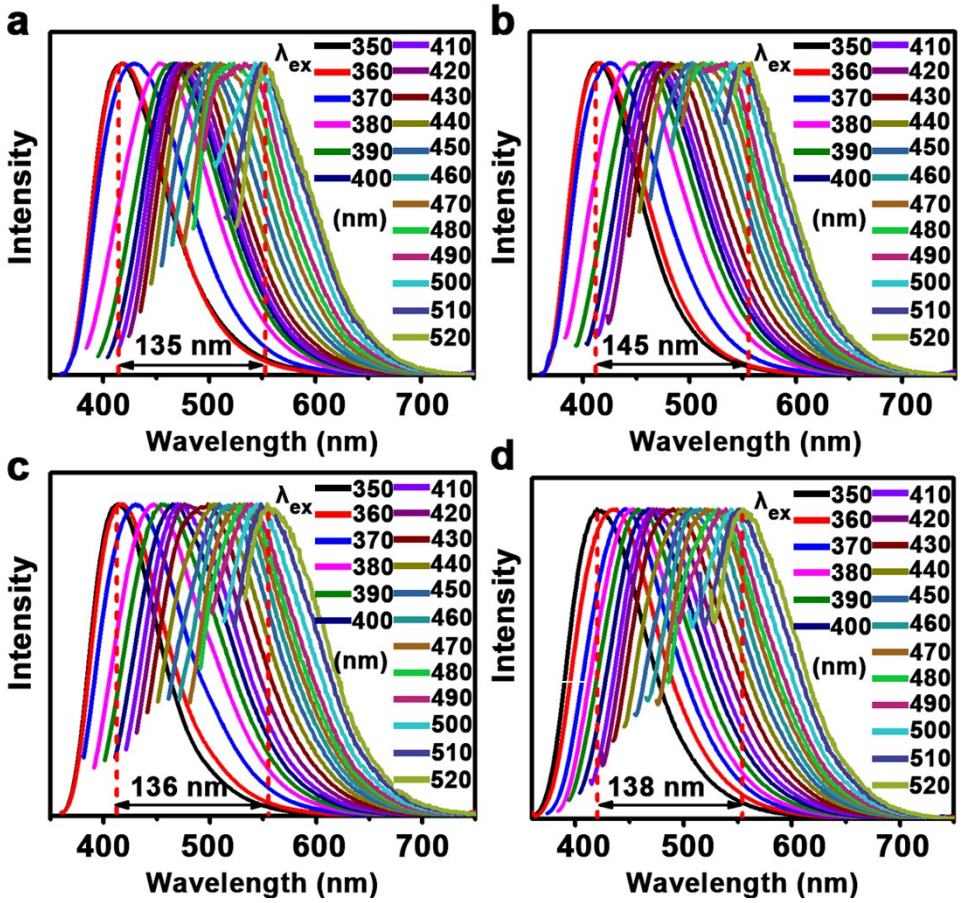

Fig. S10 Normalized PL spectra of the resultant SiNPs under different excitation wavelengths: (a) IST-SiNPs, the redshift range: 135 nm; (b) MIST-SiNPs, the redshift range: 145 nm; (c) TTIA-SiNPs, the redshift range: 136 nm; (d) MTTIA-SiNPs, the redshift range: 138 nm. The broad red-shift range (>130 nm) from ~420 to ~550 nm under serial excitation wavelengths from 350 to 520 nm, is observed in the resultant SiNPs. Furthermore, we find the electron-richer ligand would result in a relatively larger redshift range, indicating that the emission range of the SiNPs is influenced by the electronic structure of the ligand.

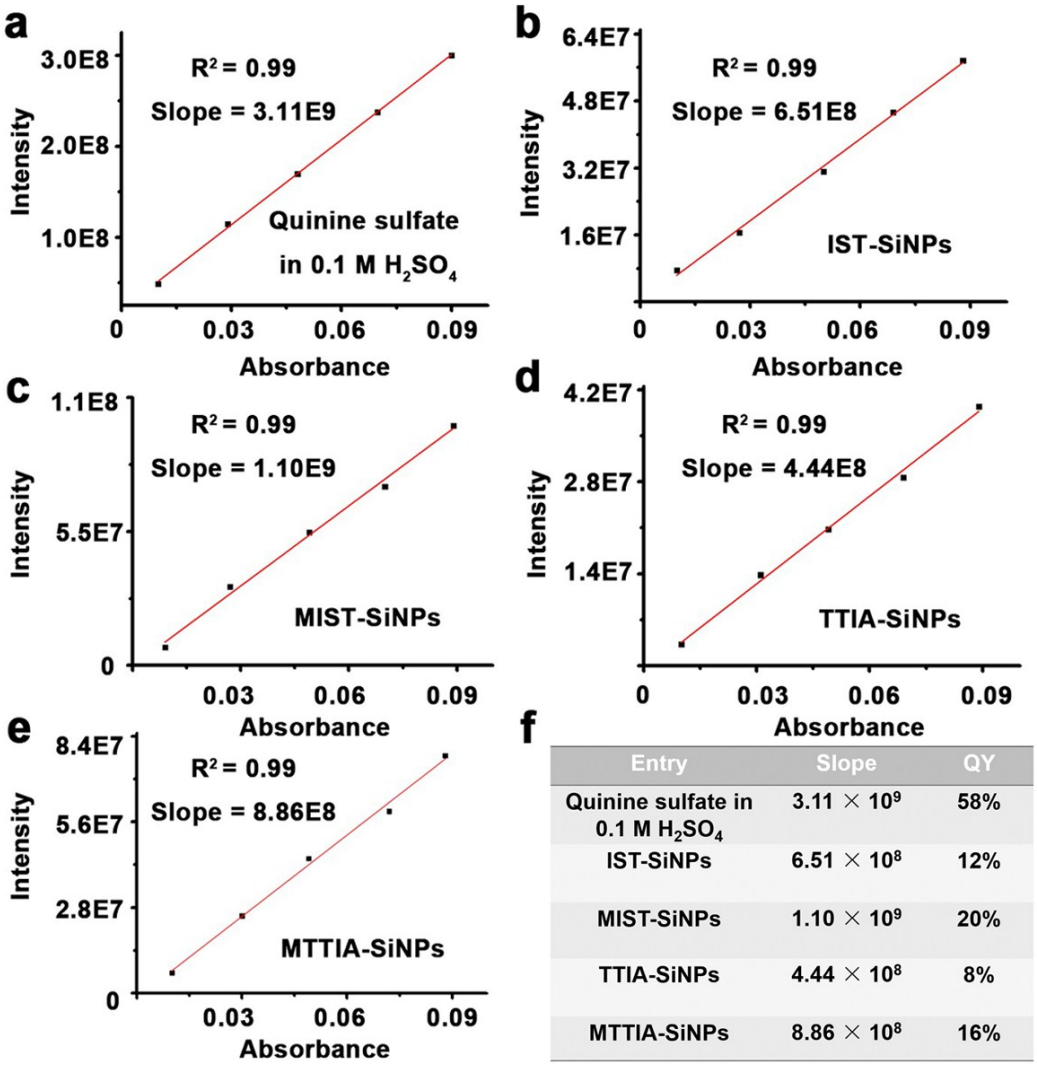

Entry	Slope	QY
Quinine sulfate in 0.1 M H_2SO_4	3.11×10^9	58%
IST-SiNPs	6.51×10^8	12%
MIST-SiNPs	1.10×10^9	20%
TTIA-SiNPs	4.44×10^8	8%
MTTIA-SiNPs	8.86×10^8	16%

Fig. S11 Photoluminescent quantum yields (PLQY) measurements of the resultant SiNPs: (a) Quinine sulfate in 0.1 M H_2SO_4 (standard). (b) IST-SiNPs. (c) MIST-SiNPs. (d) TTIA-SiNPs. (e) MTTIA-SiNPs. (f) Summary table of QYs. QYs of the SiNPs were obtained by inputting slope value (K) into the equation: $\Phi_x = \Phi_{st} (K_x/K_{st})$ (Section 1.6).

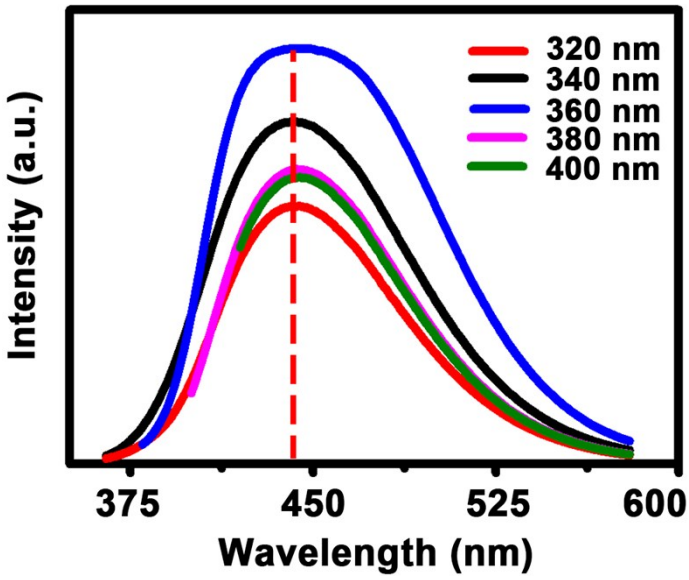

Fig. S12 PL spectra of NH_2-capped SiNPs under different excitation wavelengths. Accompanied with the increase of the excitation wavelength, the position of maximum emission wavelength is not changed, indicating excitation wavelength-independent PL property of the NH_2-capped SiNPs.

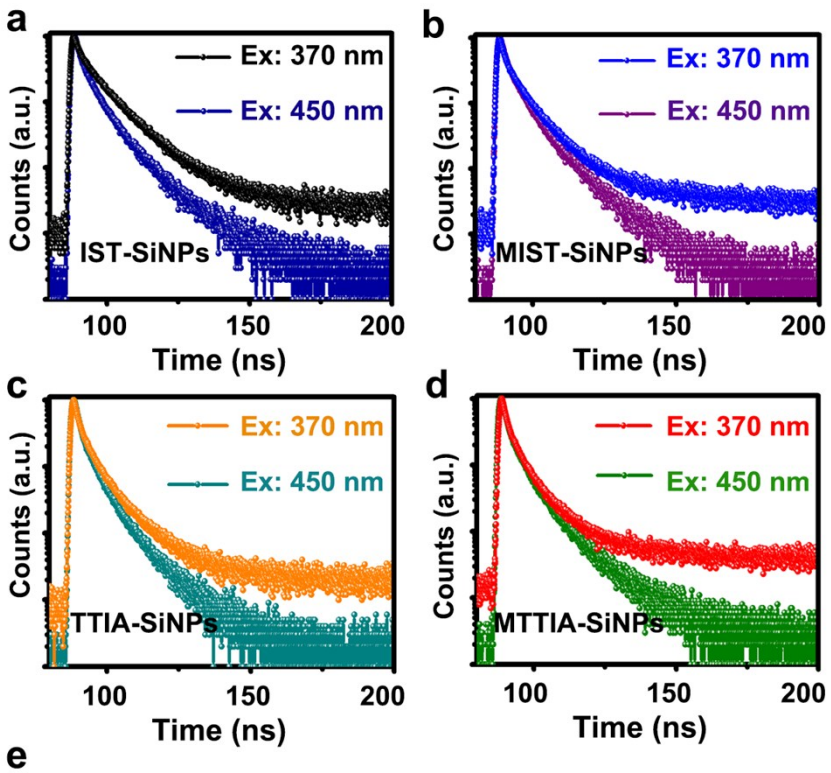

e

Excitation Wavelength	IST-SiNPs	MIST-SiNPs	TTIA-SiNPs	MTTIA-SiNPs
370 nm	11.3 ns	16.7 ns	8.7 ns	14.6 ns
450 nm	7.9 ns	8.0 ns	6.4 ns	7.0 ns

Fig. S13 PL lifetimes of resultant SiNPs under excitation wavelengths of 370 nm and 450 nm. (a) IST-SiNPs (λ_{ex} = 370 nm, λ_{em} = 430 nm; λ_{ex} = 450 nm, λ_{em} = 500 nm, 25 °C). (b) MIST-SiNPs (λ_{ex} = 370 nm, λ_{em} = 430 nm; λ_{ex} = 450 nm, λ_{em} = 500 nm, 25 °C). (c) TTIA-SiNPs (λ_{ex} = 370 nm, λ_{em} = 430 nm; λ_{ex} = 450 nm, λ_{em} = 510 nm, 25 °C). (d) MTTIA-SiNPs (λ_{ex} = 370 nm, λ_{em} = 445 nm; λ_{ex} = 450 nm, λ_{em} = 510 nm, 25 °C). (e) Summary table of PL lifetimes under different excitation wavelengths. The PL lifetimes of these SiNPs excited at 450 nm are slightly shorter than those excited at 370 nm, which is due to the mismatch of the excitation wavelength at 450 nm.[6]

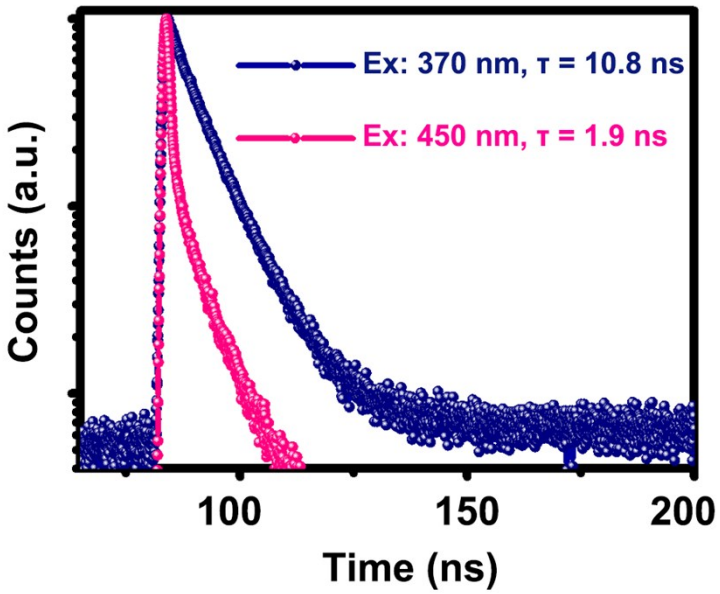

Fig. S14 PL lifetimes of excitation-wavelength-independent NH_2-SiNPs at 370-nm and 450-nm excitation. PL lifetime of NH_2-SiNPs is dramatically decreased from 10.8 ns (λ_{ex} = 370 nm, λ_{em} = 445 nm, 25 °C) to 1.9 ns (λ_{ex} = 450 nm, λ_{em} = 500 nm, 25 °C). The extremely short PL lifetime excited at 450 nm indicates that nonradiative decay is more favored than the radiative recombination, which is different from the results of ligand-decorated SiNPs, whose PL lifetimes are still maintained at ~6-8 ns under 450-nm excitation. These data suggest that the resultant ligand-decorated SiNPs feature different pathways for recombination of electrons and holes, i.e., different CT states during ligand-actived process. This ligand-actived CT process would produce the multiple energy levels in the band gap of SiNPs, and generate excitation-wavelength-dependent emission property.

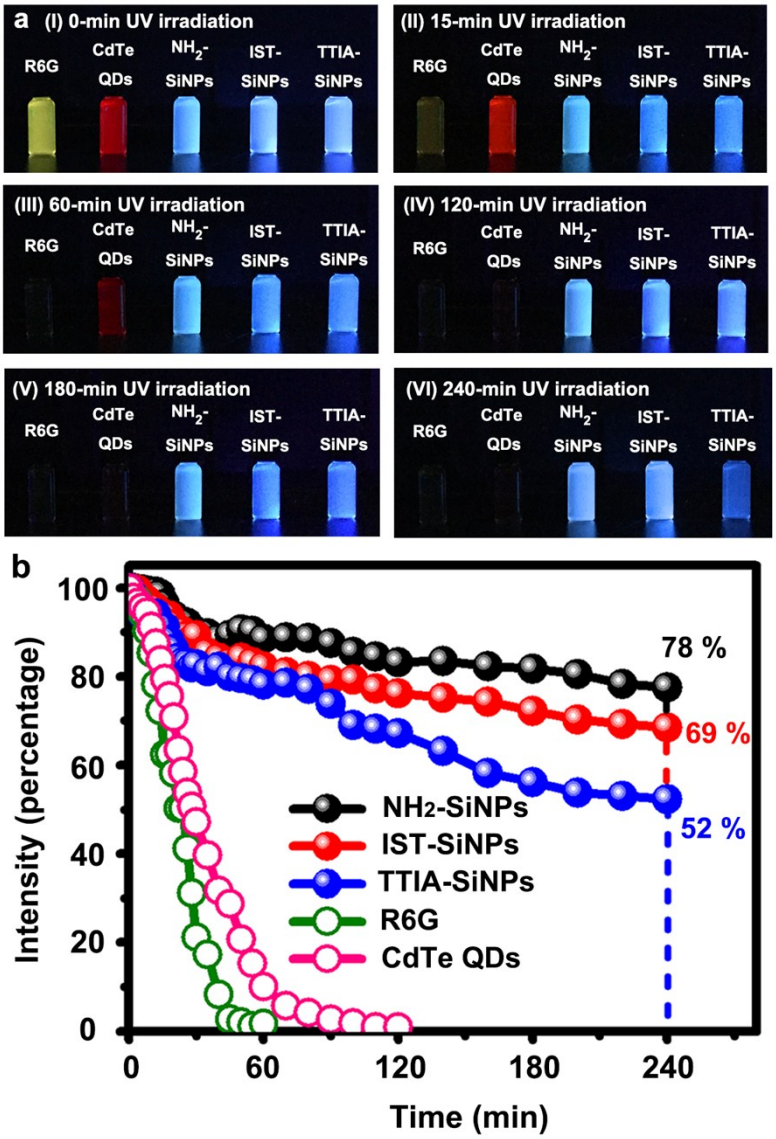

Fig. S15 (a) Fluorescent photographs of R6G, CdTe QDs, NH_2-SiNPs, IST-SiNPs, and TTIA-SiNPs. Fluorescence of R6G is evidently decreased in 15-min UV irradiation due to serious photobleaching. Fluorescence of CdTe QDs becomes negligible in 60 min owing to Te oxidation under high-power UV irradiation.[3] In comparison, IST- and TTIA-SiNPs exhibit superior photostability against long-term (4 h) high-power UV irradiation, which is similar with the reported NH_2-SiNPs featuring high photostability[3]. (b) Photostability comparison spectra. Within 240-min UV irradiation, the IST-SiNPs preserve ~70% of the initial intensity, while only ~50% of the initial intensity is maintained for the TTIA-SiNPs. The reason could mainly be attributed to the ring-opening molecular structure of TTIA. Compared with the rigid-structured IST, TTIA is less stable and prone to be decomposed under the long-term high-power UV irradiation.

References

(1) J. A. Gerbec, D. Magana, A. Washington, G. F. Strouse, *J. Am. Chem. Soc.*, 2005, **127**, 15791-15800.

(2) F. Peng, Y. Y. Su, Y. L. Zhong, C. H. Fan, S. T. Lee, Y. He, *Acc. Chem. Res.*, 2014, **47**, 612-623.

(3) Y. L. Zhong, F. Peng, F. Bao, S. Y. Wang, X. Y. Ji, L. Yang, Y. Y. Su, S. T. Lee, Y. He, *J. Am. Chem. Soc.,* 2013, **135**, 8350-8356.

(4) H. Qin, Y. Niu, R. Meng, X. Lin, R. Lai, W. Fang, X. Peng, *J. Am. Chem. Soc.,* 2014, **136**, 179-187.

(5) B. Song, Y. L. Zhong, S. C. Wu, B. B. Chu, Y. Y. Su, Y. He, *J. Am. Chem. Soc.,* 2016, **138**, 4824-4831.

(6) B. Ghosh, M. Takeguchi, J. Nakamura, Y. Nemoto, T. Hamaoka, S. Chandra, N. Shirahata, *Sci. Rep.* 2016, **6**, 36951.